

Spectroscopic and thermal analyses for the effect of acetic acid on the plasticized sodium carboxymethyl cellulose

Rania Badry^a, Hend A. Ezzat^b, Sherif El-Khodary^c, Mohamed Morsy^c, Hanan Elhaes^a, Nadra Nada^a, Medhat Ibrahim^{d,*}

^a Physics Department, Faculty of Women for Arts, Science and Education, Ain Shams University, 11757 Cairo, Egypt

^b Nano Technology Unit, Space Lab, Solar and Space Research Department, National Research Institute of Astronomy and Geophysics (Nano NRIAG), 11421 Helwan, Cairo, Egypt

^c Building Physics and Environment Institute, Housing & Building National Research Center (HBRC), 12311 Dokki, Giza, Egypt

^d Molecular Spectroscopy and Modeling Unit, Spectroscopy Department, National Research Centre, 33 El-Bohouth St., 12622 Dokki, Giza, Egypt

ARTICLE INFO

Article history:

Received 1 April 2020

Revised 24 July 2020

Accepted 3 August 2020

Available online 4 August 2020

Keywords:

CMC

UV-Vis.

FTIR

NMR

EIS

TGA

ABSTRACT

Solid polymer electrolytes (SPEs) based on sodium carboxymethyl cellulose (CMC) mixed with different percentages of acetic acid and constant percentage of glycerol (Gly) as a plasticizer, to enhance electrical properties, are prepared using casting technique. Then, the prepared SPE films are characterized using Ultraviolet-Visible spectroscopy (UV-Vis.), Fourier Transform Infrared spectroscopy (FTIR), Nuclear Magnetic Resonance (NMR), Scanning electron microscope (SEM) and Electrical Impedance Spectroscopy (EIS). Also, thermal properties of the studied SPEs are studied using Thermo Gravimetric Analyzer (TGA) and its derivative (DTA). The obtained results of UV-Vis. study indicated that the prepared samples possess three optical band gaps and that the optical band gaps decreased due to increasing acetic acid concentration up to 5 wt.%. FTIR results predict the presence of new absorption band around 1693 cm^{-1} . Acetic acid/CMC interaction is further described by ¹HNMR indicating chemical shift in carbonyl carbon ($\text{C} = \text{O}$) in some samples and disappearing of it in another samples. Meanwhile, EIS results indicated that the highest ionic conductivity obtained equals 7.64E-06 S/cm at room temperature for sample A3. Finally, TGA curves showed that the thermal stability is changed with changing acid concentration and three stages of weight loss are observed. The obtained results indicated that CMC-Gly-acetic acid SPEs is a perfect choice to be used as a solid polymer electrolyte since the electrical properties of CMC are improved.

© 2020 Elsevier B.V. All rights reserved.

1. Introduction

Following up the structural changes as a result of different factors is the main goal of spectroscopic methods of analyses [1,2]. Such method includes but not limited to UV-Vis, FTIR, XRD, NMR beside SEM techniques [3–5]. Polymeric materials are considered among so sensitive materials for chemical as well as physical treatments [6]. Accordingly, several techniques are required to study polymers in order to functionalize their applications in appropriate applications [7].

Cellulose one of the most abundant material on the earth, this fact enable cellulose derivatives to be a hot topic of research according to their abundant, biodegradable and easy handling as well as low cost [8,9]. Among these applications, nanocomposite mem-

branes were prepared from graphene-loaded with sodium alginate with enhanced isopropanol dehydration performance via a pervaporation technique [10]. Sodium alginate as a cost effective material and ecofriendly could be further utilized as a matrix for organically modified clay particles prepared by treating with p-TSA for deriving membranes that were tested for PV dehydration of IPA-water mixture [11]. Chitosan another member of polysaccharides with NH_2 group allow it for many functions is tried for membrane [12]. Graphene sheets are embedded in chitosan forming nanocomposite also act as membrane for ethanol and isopropanol dehydration via pervaporation.

The growth of new solid polymer electrolyte materials playing a very important role in developing and creating new electrochemical devices, solar cells, batteries, and gas sensors [13]. In the past, liquid electrolytes are considered as the main sources of electrochemical power due to its high ionic conductivity. But these electrolytes have a lot of drawbacks like leakage, difficulty in

* Corresponding author.

E-mail address: medahmed6@yahoo.com (M. Ibrahim).

handling liquids so it can be spillage, interact with electrodes which gradually corrodes the electrodes and hence decreases the device lifespan. Additionally, the solvent boiling point limits the temperature range of the device operation and poor electrochemical stability [14,15]. After the discovery of solid polymer electrolytes in 1973, researchers recognized that these solid electrolytes can be used instead of liquid electrolyte because they have high ionic conductivity and excellent mechanical and thermal stability [16]. Also the use of these materials (i.e. SPEs), which are considered as friends to the environment, eliminates the previous problems of liquid electrolytes as it exhibits a lot of features such as: simple preparation in different geometrical shapes, good contact between electrode and electrolyte interface, no leakage, good mechanical and adhesives properties and safety [17,18]. However, SPEs possesses a considerable defect due to their higher degree of crystallinity, but this problem can be overcome by the addition of organic or inorganic salts/acids [19]. Since the detection of the first ion-conducting polymer, namely, poly (ethylene oxide) dissolved in alkali metal salts, various types of polymers have been investigated to be used as a polymer electrolyte (PE). Research has involved natural polymers such as starch, cellulose and chitosan as they possess low- cost, availability and biocompatibility compared to synthetic polymers [20,21]. Cellulose is the most abundant Polysaccharide polymer in the environment suitable for various applications including SPE applications as it has very important properties like availability, inexpensive, biodegradable, and renewable [22–25]. The use of cellulose and its derivatives as a polymer electrolyte is noteworthy as they are predictable to bring a greener future unlike harmful and toxic materials [26,27]. Carboxymethyl cellulose (CMC) is one of the most important cellulose derivatives. CMC is known as cellulose gum and sodium carboxymethyl cellulose that can form a transparent film and own high mechanical strength. Natural polymers. Also, CMC is a naturally polysaccharide substance and used widely in many industrial applications such as food, textiles, paper, adhesives, paints, pharmaceuticals, cosmetics, and mineral processing. Also, It is a natural organic polymer that is non-toxic, renewable, available in abundance, biocompatible and biodegradable [28,29]. The aim of this work is to gain an insight for CMC and acetic acid as a polymer host and as a proton donor respectively to develop a new type of plasticized SPEs. Also, the study focuses on the electrical properties of the prepared SPEs to be applicable for electrochemical applications and optoelectronic devices. Glycerol is chosen as a plasticizer according to its ability to increase the flexibility of polymers and improve mechanical and thermal stability of the prepared samples [30–32]. Accordingly, the studied samples were subjected to different characterizing tools including UV-Vis.; FTIR; NMR, SEM, EIS and TGA.

2. Materials and method

2.1. Sample preparation

CMC is acquired from (K. Patel Chemo pharma PVT. India) with average molecular weight of 2.5×10^5 g/mol while, acetic acid is acquired from El Nasr Pharmaceutical Chemicals Co., Cairo, Egypt. Solution casting technique is used to prepare our CMC-Gly-acetic acid based SPEs. One gram of CMC (weighted by a digital balance) is dissolved in distilled water and stirred with magnetic stirrer and bar for 8 h until CMC powder is totally dissolved. Constant percentage of glycerol (wt. 40%) is added to CMC solution and stirred for 1 hour. Then different weight percentages (start from 2.5 to 15 wt.%) of acetic acid are added to the CMC-Gly-solution and stirred until there is no phase change and it became homogeneous. The mixtures are then cast into glass petri dishes and left to dry at room temperature for 3 to 5 days depending on the acetic acid

Table 1

Designation and composition of the CMC-Gly- acetic acid SPE films.

Acetic acid (wt.%)	Plasticizer (Glycerol)	Water (ml)	CMC (g)	Sample
0.0				A1
2.5				A2
5.0	40	75	1	A3
7.5				A4
10.0				A5
12.5				A6
15.0				A7

concentration. The samples are abbreviated according to acetic acid content as depicted in Table 1.

2.2. Characterization of solid polymer electrolyte films

2.2.1. UV-Visible spectroscopy (UV-Vis.)

The UV-Visible absorption spectra of CMC-Gly-acetic acid SPEs are recorded in the wavelength range from 200 to 1000 nm, using a double beam spectrophotometer (JASCO model V-670 UV-Vis-NIR) at Spectroscopy Department, National Research Centre (NRC), Cairo, Egypt.

2.2.2. Fourier transform infrared spectroscopy (FTIR)

The absorption spectra of the prepared SPE films are conducted using attenuated total reflection (ATR) FTIR spectroscopy, Bruker VERTEX 70, at Spectroscopy Department, National Research Centre (NRC), Cairo, Egypt. The spectra are recorded in the mid infrared region of the spectral range with a resolution of 4 cm^{-1} to characterize the presence of different functional groups in CMC-Gly-acetic acid SPE films.

2.2.3. Nuclear magnetic resonance (NMR) spectroscopy

Nuclear magnetic resonance (NMR) that was operated by JEOL ECA-500 MHz at National Research Centre (NRC) to obtain both ^1H NMR and ^{13}C NMR. The ^1H NMR run was operated at 500 MHz and 125 MHz at ^{13}C NMR in (ppm) range. Samples were dissolved in (40.00 μl) deuterated water (D_2O) and applied to run with 16 scans for ^1H NMR and applied to run with 2000 scans ^{13}C NMR.

2.2.4. Scanning electron microscope (SEM)

The surface morphology of the studied films was examined by Scanning Electron Microscope (SEM) model FEI, Inspect S, instrument operating at 100KV, at Building Physics and Environment Institute, Housing & Building National Research Center (HBRC), Dokki, Giza, Egypt.

2.2.5. Electrical impedance spectroscopy (EIS)

For SPEs based on plasticized CMC/acetic acid, conductivity is measured via electrical impedance spectroscopy using HIOKI 3532–50 LCR Hi-Tester that is connected to a computer, at Building Physics and Environment Institute, Housing & Building National Research Center (HBRC), Dokki, Giza, Egypt.

The conductivity of the plasticized SPEs is measured in a frequency range 50 Hz: 1 MHz at several temperatures started from 298 to 388 K. The SPE films are cut into suitable size and sandwiched between two stainless-steel blocking electrodes of the sample holder that connected to the LCR tester.

2.2.6. Thermo gravimetric analysis (TGA)

Thermal characteristics of polymers are studied using thermo gravimetric analyzer (TGA) and its derivative (DTG). Thermal analyses are conducted using TGA thermal analyzer (STD-Q600, USA) at a heating rate of $5 \text{ }^\circ\text{C} / \text{min}$ from $24 \text{ }^\circ\text{C}$ to $511 \text{ }^\circ\text{C}$ in nitrogen atmosphere to predict the mass loss.

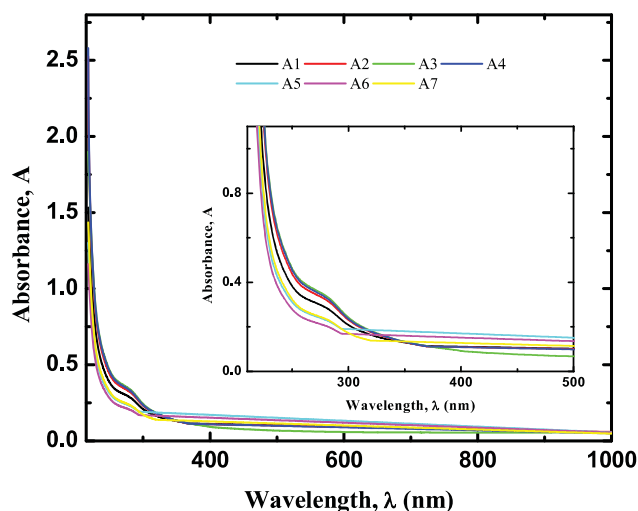


Fig. 1. Optical absorption spectra of SPE films based on CMC and CMC doped with acetic acid appreciated as presented in Table 1 in the wavelength range from 200 nm to 1000 nm.

Table 2

Refractive index values for pure CMC and CMC doped with different concentrations of acetic acid and their indirect allowed band gap values.

Structure	N	E ₁ (eV)	E ₂ (eV)	E ₃ (eV)
A1	2.34	1.52	3.24	4.7
A2	2.35	2.5	3.18	4.52
A3	2.52	1.55	2.57	4.46
A4	2.34	1.99	3.22	4.51
A5	2.49	2.69	2.69	4.79
A6	2.50	2.63	2.63	4.91
A7	2.45	2.82	2.82	4.8

3. Results and discussion

3.1. UV-Vis absorption spectra analysis

The absorption spectra of SPEs based on CMC/acetic acid in the UV-Vis. spectral region are recorded in the wavelength ranging from 200 nm to 1000 nm as presented in Fig. 1. The studied system shows a shift (red) toward the longer wavelength region with increasing the content of acetic acid in the prepared SPEs. The absorption shoulder shift refers to the complexation occurs between CMC and acetic acid. Additionally, it refers to the changes happens for the optical energy gap because of changing the degree of crystallinity of CMC [33]. The absorption shoulder observed at 225 nm may be attributed to $n \rightarrow \pi^*$ transition of electrons. The changes occurred in the absorption edge due to the addition of acid is presented in Table 2 in terms of the band gap. As presented in the table that the absorption edge value is decreased with increasing acid concentration up to 5 wt.% afterwards it increased again.

3.2. Optical energy gap of CMC/acetic acid SPEs

As indicated in Fig. 1 that the absorption edge of CMC undergoes a red shift with acetic acid addition. This shift indicated that the gap width is decreased due to increasing acetic acid. As reported by the Beer-Lambert law that the absorption coefficient is related to the absorbance of the material through [34]:

$$\alpha = 2.303(A/L) \quad (1)$$

Where, α is the absorption coefficient, A is the absorbance of the studied samples and L is the thickness of the prepared films. Optical transitions between the conduction and valence bands

starts when the material absorbs photons of energy ($h\nu$) equal to or greater than the energy difference between the characteristic bands. As reported by Davis and Mott that the values of the optical energy gap together with the type of electronic transition can be determined through using the following equation [35]:

$$(\alpha h\nu)^n = B(h\nu - E_g) \quad (2)$$

where, $h\nu$ is the incident photon energy, E_g is the optical energy gap and n is a constant refers to the type of transitions where it takes values of 2, 2/3, 1/2 and 1/3 for direct allowed, direct forbidden, indirect allowed and finally indirect forbidden transitions respectively [36,37].

Also, Davis and Mott reported that the two different types of transitions, direct and indirect allowed, can be determined near the edge of the fundamental absorption band. This energy gaps can be determined by plotting both $(\alpha h\nu)^2$ and $(\alpha h\nu)^{1/2}$ as a function of energy. The type of transition between the valence band and the conduction band can be determined using the David and Mott equation and making the derivative for the equation with respect to the photon energy. After that, divide the two equations on each other $(\alpha h\nu / D \alpha h\nu)$ then plotting the relation between them and the incident energy. As a result, it is concluded that the type of transition is indirect allowed transition since n equals 1/2 which also reported in the literature. Fig. 2 depicts the variation of $(\alpha h\nu)^{1/2}$ for all samples with the incident energy.

By extrapolating the straight portions of the curve on the x-axis the indirect allowed energy gap values, where the electrons cross the conduction band at different K- space, can be obtained for all samples [38]. It is found that the optical energy gap of pure CMC is influenced and decreased by acetic acid presence. As presented in the figure that the prepared samples possess more than one band gap.

Table 2 presents the different values of the optical band gap for all samples. Where, it is observed that this new type of SPEs based on CMC/acetic acid possesses three optical band gaps due to the amorphousity of the prepared samples. The first band gap values are observed at 1.52, 2.5, 1.55, 1.99, 2.69, 2.63 and 2.82 eV for samples A1, A2, A3, A4, A5, A6 and A7, respectively. Meanwhile, the second optical band gap are observed at 3.24, 3.4, 2.57, 3.22, 3.37, 3.71 and 3.56 eV respectively for the same sequence. Finally, the third band gap are observed at 4.7, 5.426, 4.48, 4.57, 4.69, 4.91 and 4.8 eV for samples A1, A2, A3, A4, A5, A6 and A7, respectively. Additionally, it is concluded that the sample A3 is the best one as it possesses the lowest value of band gap and that the first band gap is the real band gap as it requires minimum energy for electron transport between the two bands. The reason for such a decrease in the optical energy gap may be due to the formation of chemical bonds between the CMC chain and acetic acid. Also, this decrease in the optical band gaps makes this type of SPEs very efficient for electrochemical applications and optoelectronics [37].

3.3. The dependence of the refractive index of pure CMC on acetic acid concentration

In the field of developing optically polymeric materials, the index of refraction plays a significant and effective role as it is one of the most important factors in designing new dispersion devices for all types of spectra and in optical systems of communications [33–40]. It is stated that the refractive index (n) of an optical material is a dimensionless quantity that describes how the electromagnetic radiation propagates through the polymeric materials under study and it can be calculated in terms of energy gaps E_g using equation:

$$\frac{n^2 - 1}{n^2 + 2} = 1 - \sqrt{\frac{E_g}{20}} \quad (3)$$

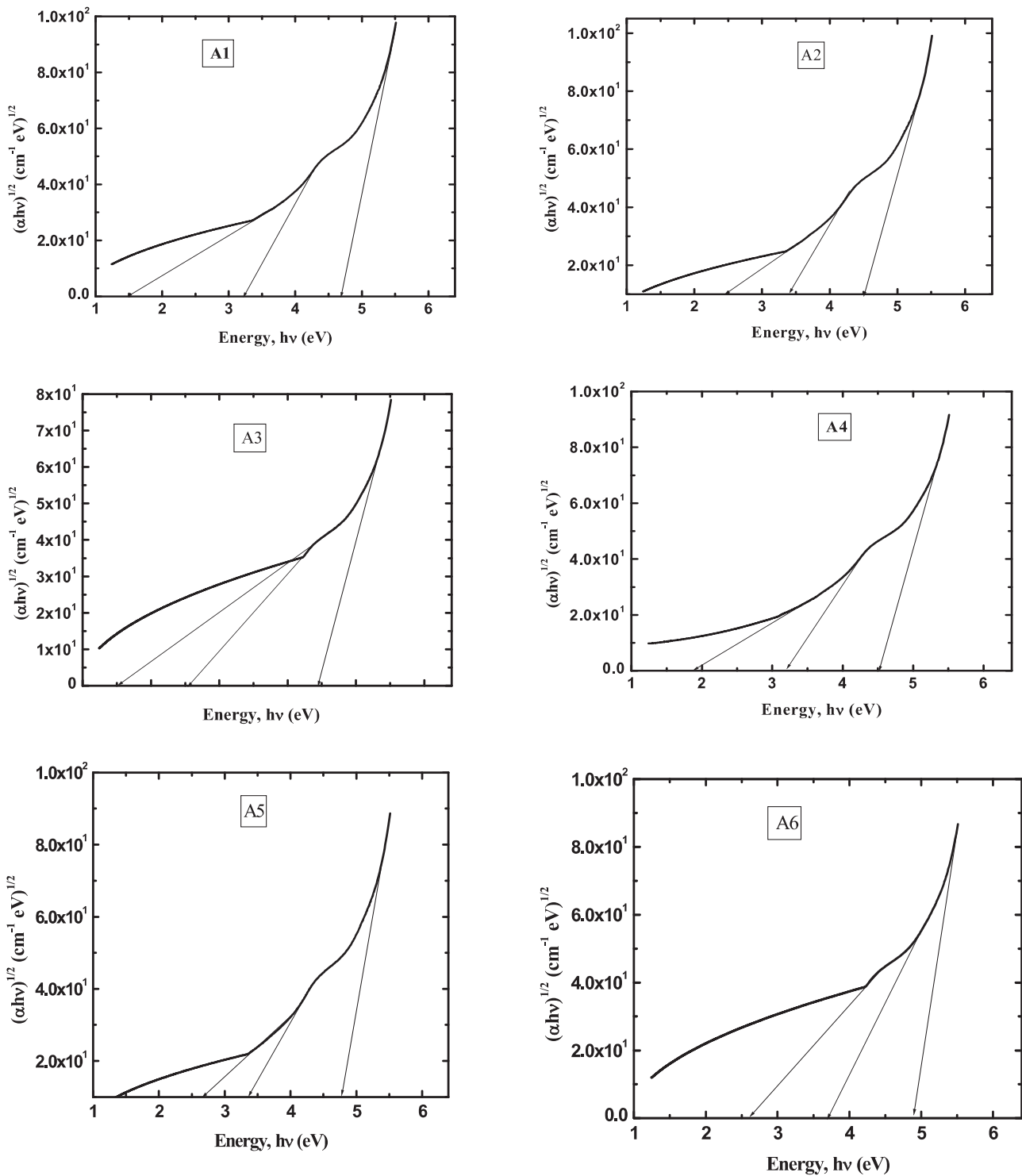


Fig. 2. Relation between $(\alpha h\nu)^{1/2}$ and photon energy ($h\nu$) for pure CMC and CMC doped with different concentrations of acetic acid as indicate in Table 1.

Table 2 presents the variations of CMC refractive index due to changing acetic acid content in the prepared films. It is observed that the values of the index of refraction of pure CMC and that of doped CMC are changed with increasing acetic acid. Where, the CMC refractive index changes from 2.34 to 2.35, 2.52, 2.34, 2.49, 2.50 and 2.45 respectively by changing the acid concentration from 2.5 wt.% up to 15 wt.%. As presented in the table, the highest refractive index belongs to the sample A3.

3.4. FTIR spectroscopy

Fig. 3 shows the FTIR absorption spectrum of pure CMC in the mid infrared region. The spectra are further assigned as indicated in Table 3 and according to the previous work the band assignment is accomplished [41,42]. From the figure, a broad absorption band is observed at 3333 cm^{-1} that is due to O–H stretching of the hydroxyl group. Meanwhile, the bands observed at 2922 cm^{-1}

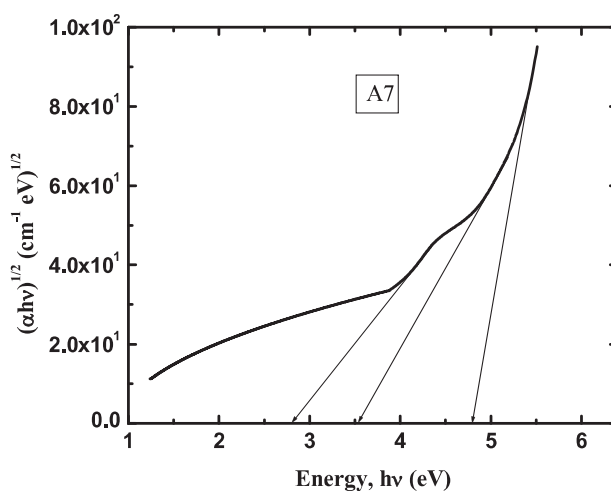


Fig. 2. Continued

Table 3

FTIR band assignment for pure CMC and CMC doped with 2.5wt%, 5wt%, 7.5wt%, 10wt%,12.5wt% and 15wt% acetic acid.

Wavenumber (cm ⁻¹)							Band Assignment
A1	A2	A3	A4	A5	A6	A7	
3333	3332	3391	3367	3358	3360	3390	O-H stretching
2922	2922	2920	2922	2922	2922	2918	C-H symmetrical stretching
2881	2878	2880	2878	2880	2880	2883	C-H asymmetrical stretching
1762	1763	1770	1755	1753	1750	1751	C = O group
-	1693	1692	1691	1691	1691	1696	COO group
1587	1589	1587	1590	1589	1590	1586	COO ⁻ stretching
1414	1414	1414	1414	1414	1414	1415	O-H stretching
1321	1320	1319	1320	1320	1320	1320	C-H stretching
1270	1270	1268	1270	1269	1269	1265	C-O symmetrical stretching
1105	1105	1104	1106	1106	1105	1102	C-O-C
1024	1024	1022	1027	1025	1025	1022	C-O stretching
919	918	-	919	918	918	-	O-H out of plane bending

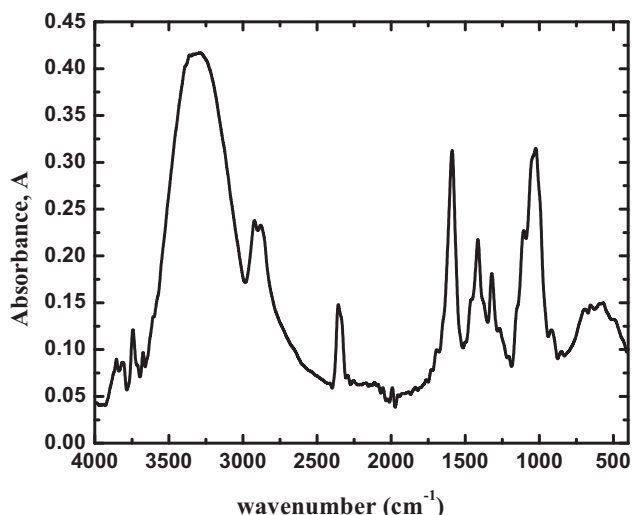


Fig. 3. FTIR spectrum of pure CMC.

and 2881 cm⁻¹ are attributed to the C-H asymmetrical stretching of CH₂ and the C-H symmetrical stretching of CH₂, respectively. However, the bands at 1762 cm⁻¹ and 1587 cm⁻¹ can be assigned for C = O group of the carboxylic group and the COO⁻ stretching of the carboxylic group, respectively.

Additionally, the band observed at 1414 cm⁻¹ is assigned to the O-H stretching of CMC, the band at 1321 cm⁻¹ is related to the C-H stretching in the methyl group and the band at 1270 cm⁻¹ is due to the C-O symmetric stretching. Additionally, the absorption band characteristic for the C-O-C symmetric and asymmetric stretching appeared at 1105 cm⁻¹ and 919 cm⁻¹ could be assigned to the C-O stretching of CH₂OCH₂ and O-H out of plane bending respectively.

Fig. 4 shows the FTIR spectra of pure CMC and that of CMC doped with acetic acid. The influence of acetic acid on the molecular structure of carboxymethyl cellulose sodium is also presented in table (3) where the existence of acetic acid in SPE films causes a shift in the band at 3333 cm⁻¹ of pure CMC with increasing the concentration up to 5 wt.%, 7.5 wt.%, 10 wt.%, 12.5 wt.% and 15 wt.% and becomes at 3391 cm⁻¹, 3287 cm⁻¹, 3358 cm⁻¹, 3360 cm⁻¹ and 3390 cm⁻¹ respectively as shown in Fig. 4.

Also, there is a new band appeared at 1693 cm⁻¹, 1692 cm⁻¹, 1691 cm⁻¹, 1691 cm⁻¹ and 1696 cm⁻¹ which may be attributed to the presence of COO⁻ stretching of acetic acid. Meanwhile, the band observed at 1762 cm⁻¹ which is due to the C = O stretching of the hydroxyl group is disappeared with the increase of acetic acid concentration to 5 wt.%, 7.5 wt.%, 10 wt.%, 12.5 wt.% and 15 wt.%. Furthermore, the intensity of the COO⁻ stretching band at 1587 cm⁻¹ of pure CMC is decreased with increasing the concentration up to 5 wt.% and then starts to increase as a result of the addition of more acetic acid which is in agreement with the results of UV-Vis. study. The obtained results of FTIR indicated that the COOH protons of acetic acid becomes free ions and

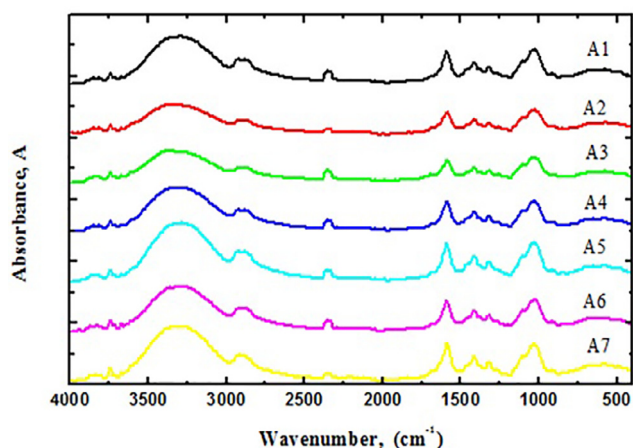


Fig. 4. FTIR spectra of pure CMC and CMC doped with different concentrations of acetic acid.

a strong complexation between CMC and acetic acid takes place [43]. The observed shift in the CMC characteristic bands refers to the changes occurred in the molecular structure of CMC because of acetic acid addition.

3.5. NMR spectroscopy

For CMC pure as shown in Fig. 5, ^1H NMR could be assigned to the following resonant regions: protons represented by two peaks at δ ppm = 3.107 and 3.254 for alcoholic hydroxyl groups located on the sugar moiety. After that δ ppm = 03.4: 04.1 are for the methine sugar protons of the moiety. After that around δ ppm = 05.1 the phenolic O–H protons appeared under the solvent broad band of D_2O .

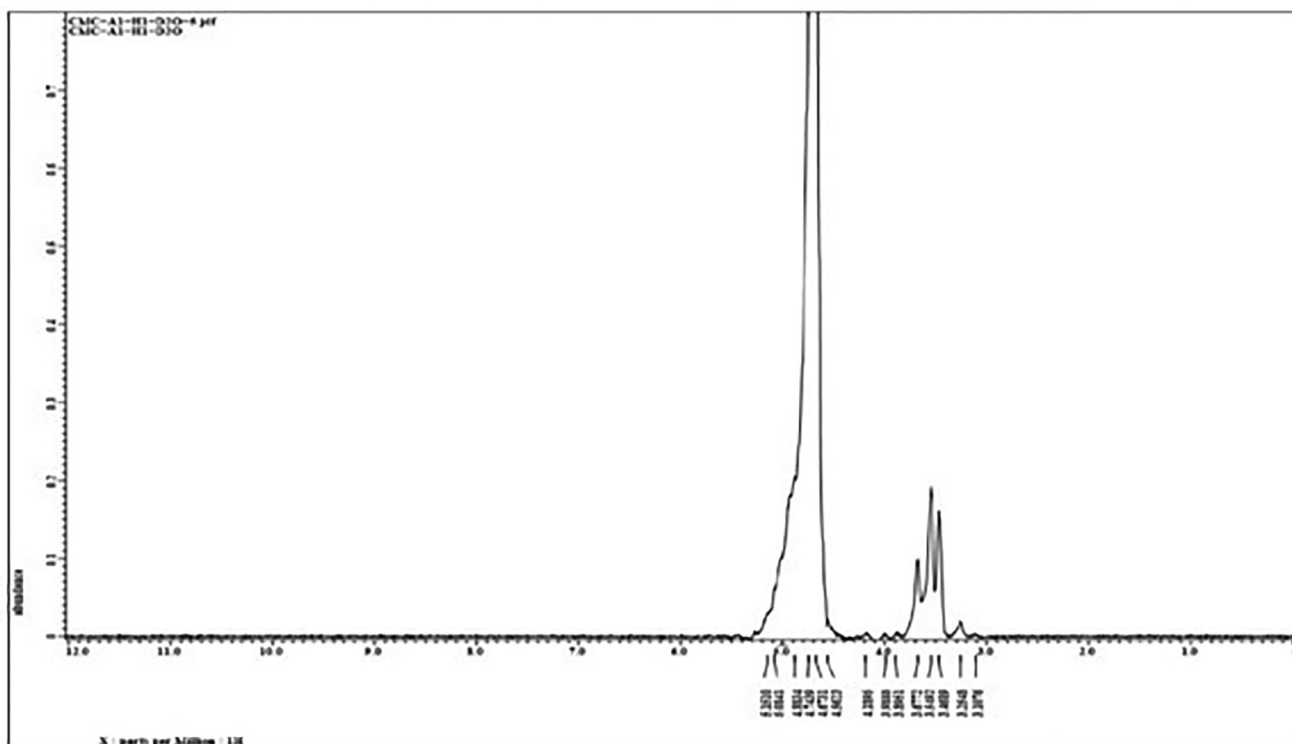


Fig. 5. ^1H NMR for CMC pure dissolved in D_2O deuterated solvent worked at 500 MHz with range from 0 to 10 ppm.

The ^{13}C NMR for pure CMC as in Fig. 6, peaks could be classified into three major regions: the most shielded sp^3 carbon atoms of the aliphatic carbon atoms shown at δ ppm: 62.7 – 72.78. The medium deshielded sp^2 carbon atoms of the aromatic ring carbon atoms have a broad band at δ ppm: 102.51. These variations in the chemical shift are due to the attachment of high electronegative atoms to the aromatic rings, such as oxygen, which increase the deshielding effect on these particular carbon atoms. The highly deshielded sp^2 carbonyl carbon atoms could be represent the extremely deshielded aldehyde carbonyl carbon atoms the true carbonyl carbon atom $\text{C} = \text{O}$ are displayed at δ ppm = 178.38.

The interaction with acetic acid were identified in ^1H NMR of sample A3 and in ^1H NMR of sample A7 that appeared in Figs. 7 and 8, as COCH_3 group of CMC with acetic acid peak at 1.760 and at 1.768 ppm. Similarly, in ^{13}C NMR for the A3 and A7 that documented in Figs. 9 and 10, there are a chemical shift in peaks of carbonyl carbon atom $\text{C} = \text{O}$ from 178.38 ppm to 173.808 ppm for A3 and disappearing of it in A7 sample, also appearing of peak at 161.427 ppm for A3 and at 166.349 ppm which also represent the interaction of acetic acid and CMC.

3.6. Scanning electron microscope

The studied samples were then subjected to SEM investigation in order to point out what their surface features. Accordingly, the surface morphologies of the SPEs films based on CMC/acetic acid are presented in Fig. 11. It was observed that the there are some sedimentation as indicated in sample A2, A5. The surface morphologies of the remaining samples indicated that, the studied CMC/acetic acid show smooth and compact structure.

3.7. Electrical impedance spectroscopy

3.7.1. Conductivity results

The ionic conductivity of CMC-Gly-acetic acid SPEs is presented in Fig. 11. As the conductivity depends on different factors includ-

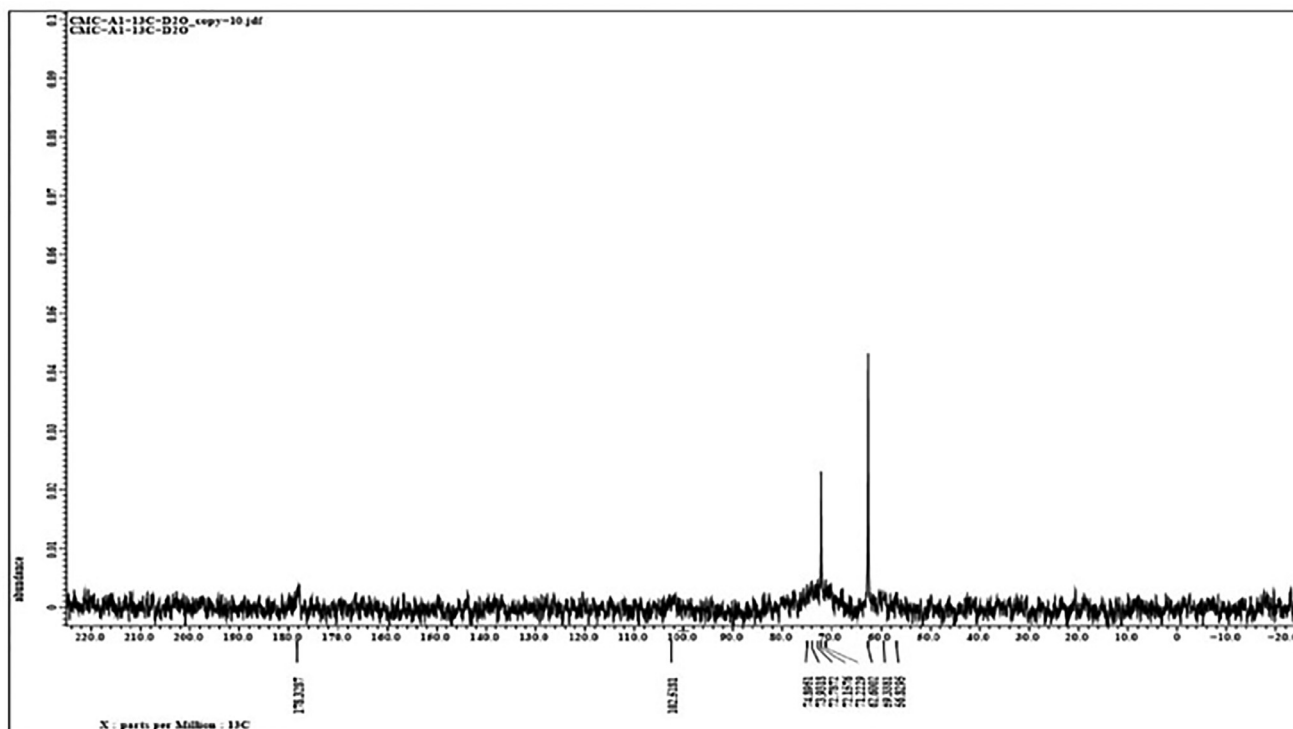


Fig. 6. ¹³C NMR for CMC pure dissolved in D₂O deuterated solvent worked at 125 MHz with range from 0 to 200 ppm.

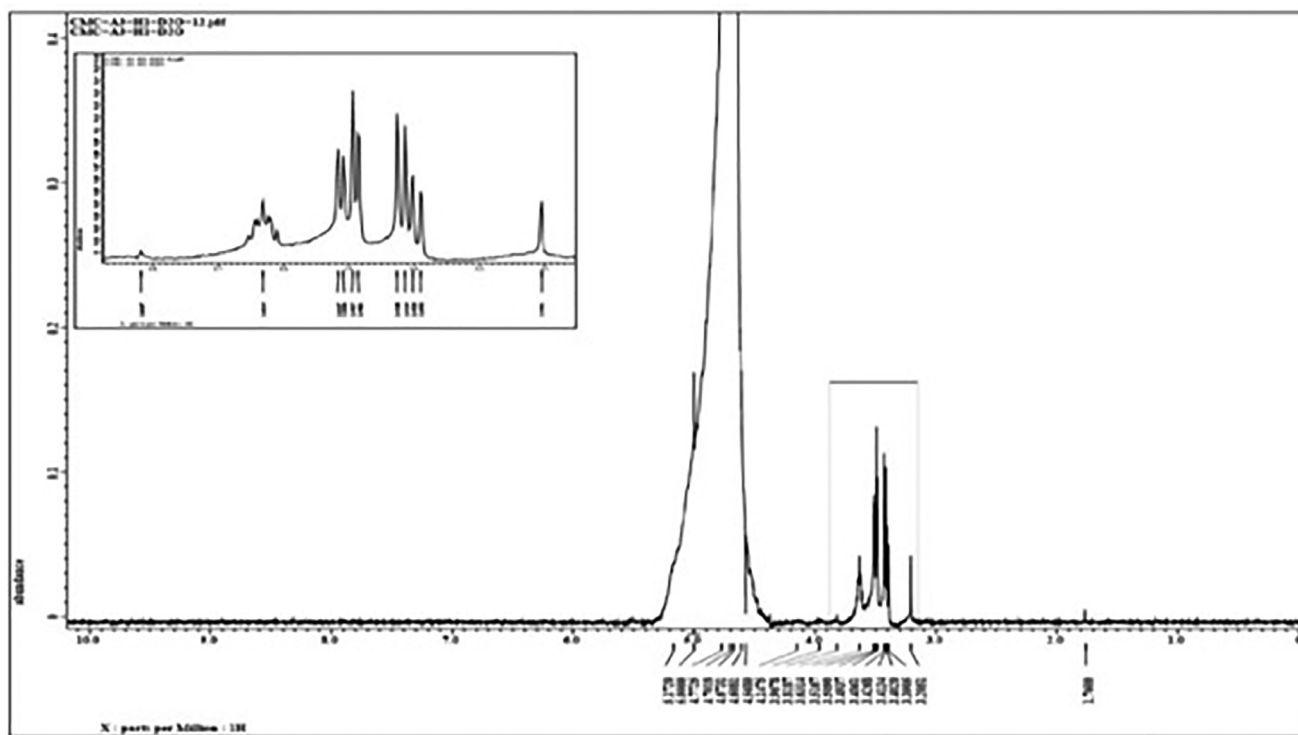


Fig. 7. ¹H NMR for CMC with acetic acid (A3) dissolved in D₂O deuterated solvent worked at 500 MHz with range from 0 to 10 ppm.

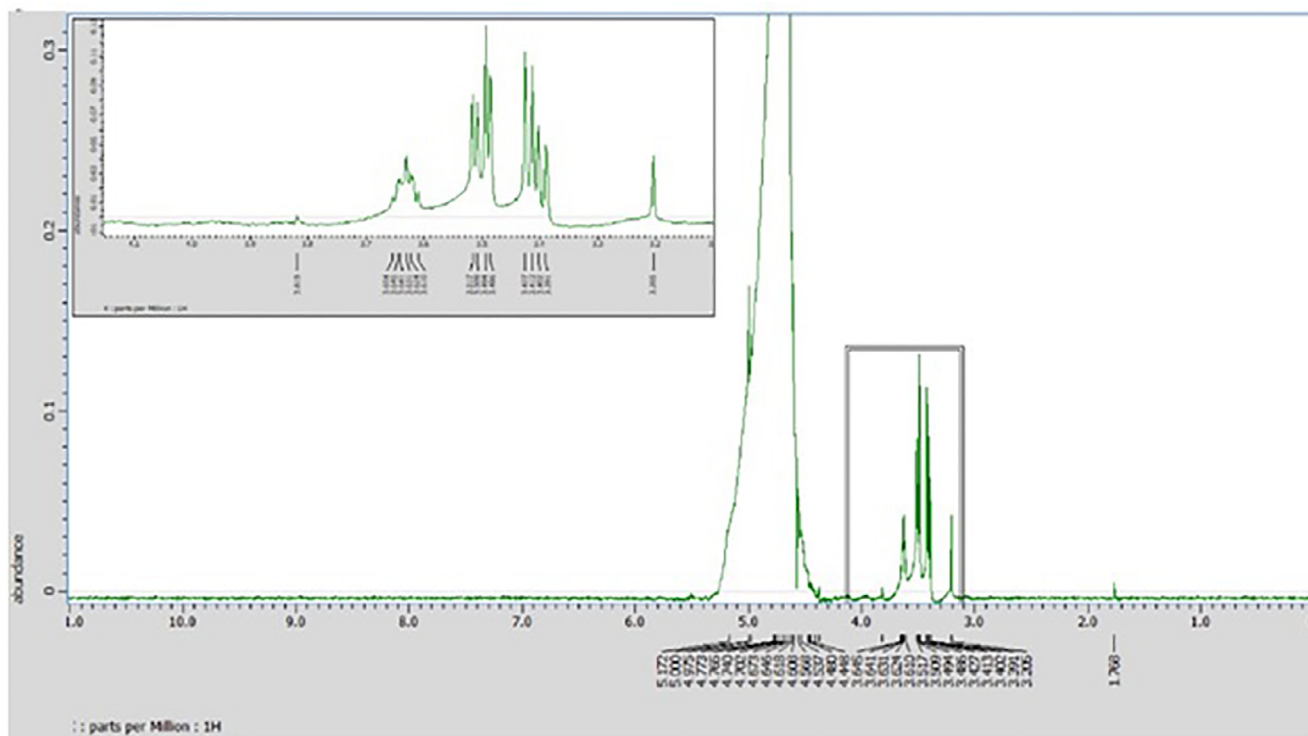


Fig. 8. ^1H NMR for CMC with acetic acid (A7) dissolved in D_2O deuterated solvent worked at 500 MHz with range from 0 to 10 ppm.

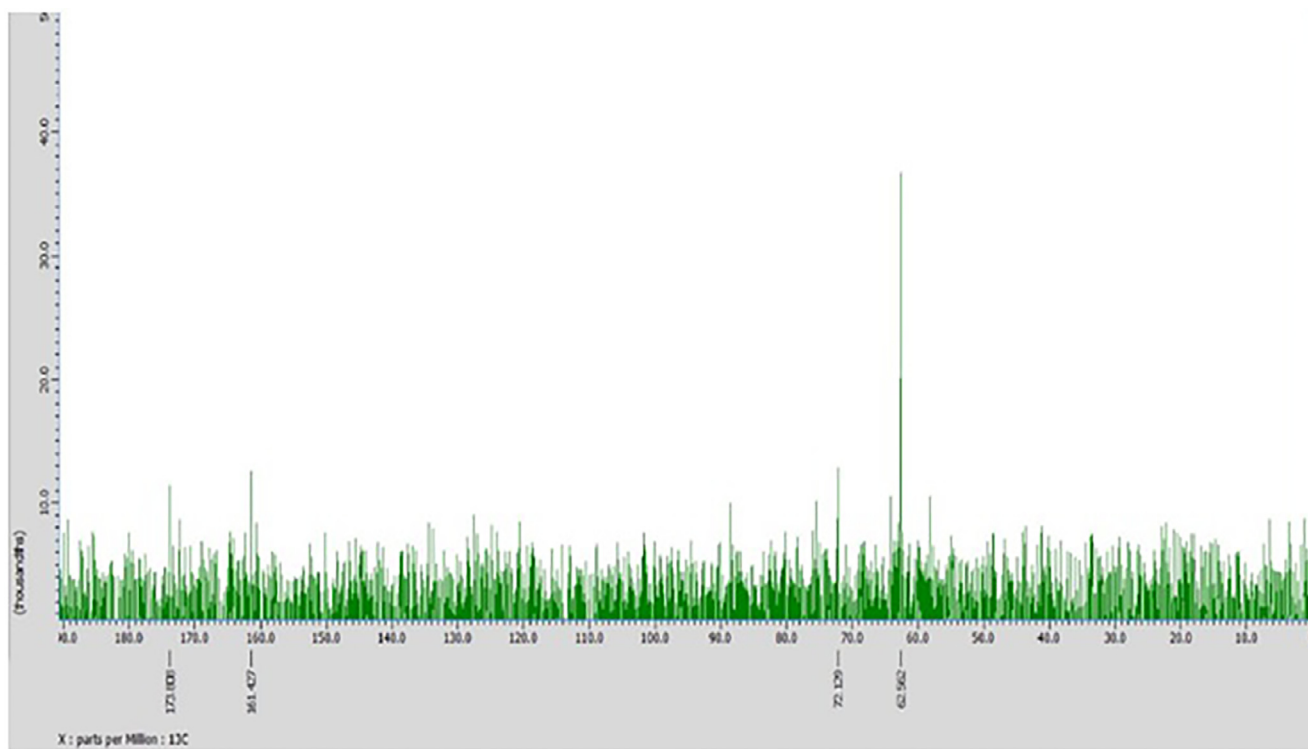


Fig. 9. ^{13}C NMR for CMC with acetic acid (A3) dissolved in D_2O deuterated solvent worked at 125 MHz with range from 0 to 200 ppm.

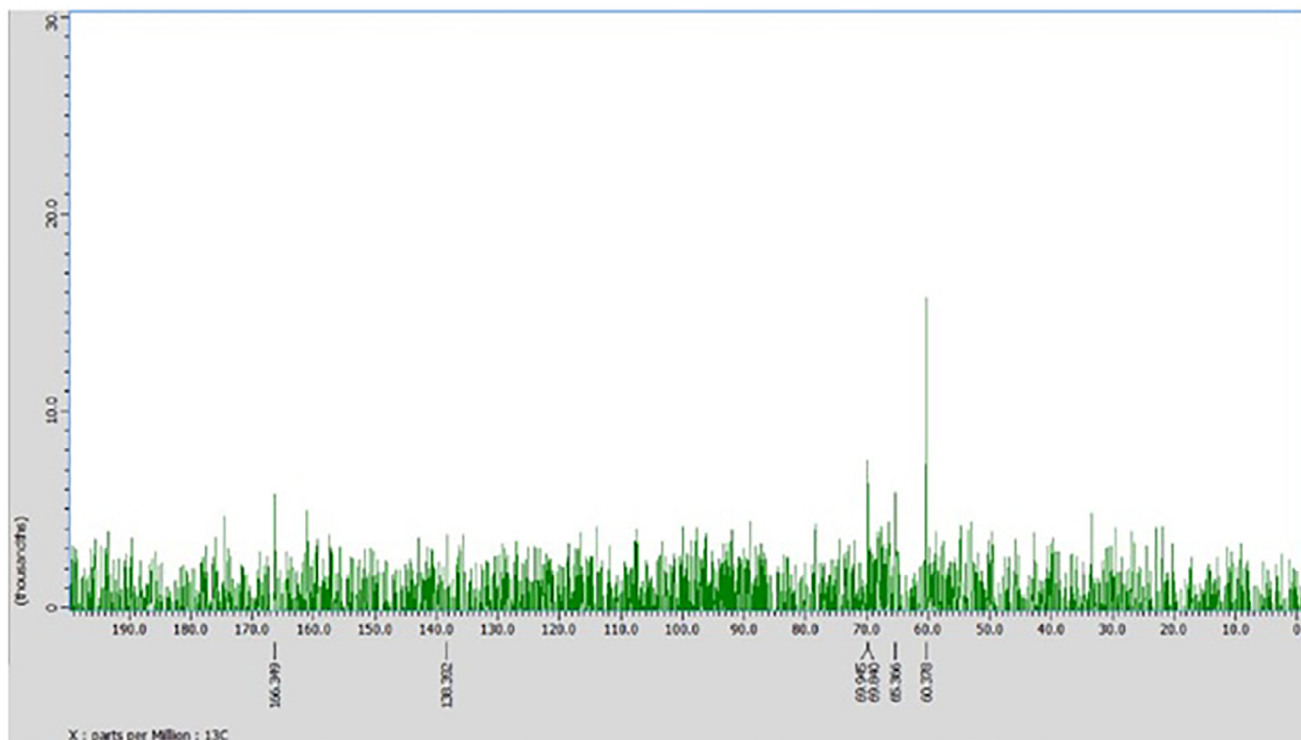


Fig. 10. ^{13}C NMR for CMC with acetic acid (A7) dissolved in D_2O deuterated solvent worked at 125 MHz with range from 0 to 200 ppm.

Table 4

The ionic conductivity and activation energy of pure CMC and CMC doped with different concentrations of acetic acid at room temperature.

Structure	AC conductivity (S/cm)	Activation Energy (eV)
A1	5.89E-07	0.8280
A2	1.91E-06	0.7887
A3	7.64E-06	0.6087
A4	2.39E-06	0.9064
A5	1.43E-06	0.9480
A6	1.21E-06	0.9739
A7	1.06E-06	0.9864

ing temperature, concentration of the dopant ions and the type of charge carriers [43], the conductivity of the prepared SPEs is calculated using equation:

$$\sigma = t/R_b A \quad (4)$$

Where, t is the thickness of the SPE film (cm); A is the electrode-electrolyte area of the film (cm^2) and R_b is the bulk resistance.

Fig. 12 shows the variation of the conductivity with acid concentration of the prepared SPEs. As shown in the figure that the AC conductivity at ambient temperature increases from 5.89E-07 S/cm of pure CMC (sample A1) to 7.64E-06 S/cm of the sample containing 5 wt.% of acetic acid (sample A3). The conductivity increased with increasing acid concentration until reach to a maximum value and then starts to decrease see Table 4. Table 5 shows the highest values of AC conductivity of CMC/other polymers doped with other salts/acids obtained by other researchers at room temperature. Where, the table shows that the obtained values of conductivity is comparable to that of the present work. These results showed that CMC, as other polymers, can host as a good proton conductor for application in electrochemical devices such as rechargeable proton batteries.

As mentioned early in ref. [43,44] that the reason for increasing the conductivity is that the ionic mobility increases with the

Table 5

AC conductivity compared with that obtained from literature at room temperature.

Structure	AC conductivity (S/cm)	Ref.
Methyl cellulose-NH ₄ F	6.40E-07	[3]
CMC- OA	2.11E-05	[5]
Chitosan- AA	1.40E-09	[6]
CMC- NH ₄ F	2.68E-07	[46]
CMC-Gly- acetic acid	7.64E-06	Present work

addition of acetic acid which is directly proportional to the conductivity. This increase in conductivity means that the amorphous regions increases within the SPEs. Also, it may be due to the high dispersion of H^+ because of the interaction between CMC and acetic acid that leads to the increment of conductivity. The conductivity starts to decrease after the addition of more than 5 wt.% acetic acid and this is due to the formation of ion clusters as the association of ions increases by the addition of more acetic acid [41,42]. These results are in good agreement with that of UV-Vis. and FTIR studies. Where, the conductivity enhancement is attributed to the complexation has been occurred between CMC and acetic acid. Additionally, these changes mean that the electronic distribution within CMC is changed due to the addition of acetic acid which confirmed that the prepared SPEs can be used in the fabrication of optoelectronic devices.

3.7.2. Temperature dependence of ac conductivity

The dependence of conductivity upon temperature is also studied to predict the behavior of ions upon heating and to discuss the mechanism of conductivity of polymeric materials [42]. Fig. 13 presents the relation between $\log \sigma$ and $1000/T$ for all samples in the temperature range from 298 K to 388 K. The figure shows that the ionic conductivity of the studied SPE films is increased with increasing temperature and follow a linear relationship. The reason for increasing the conductivity may be attributed to the increase

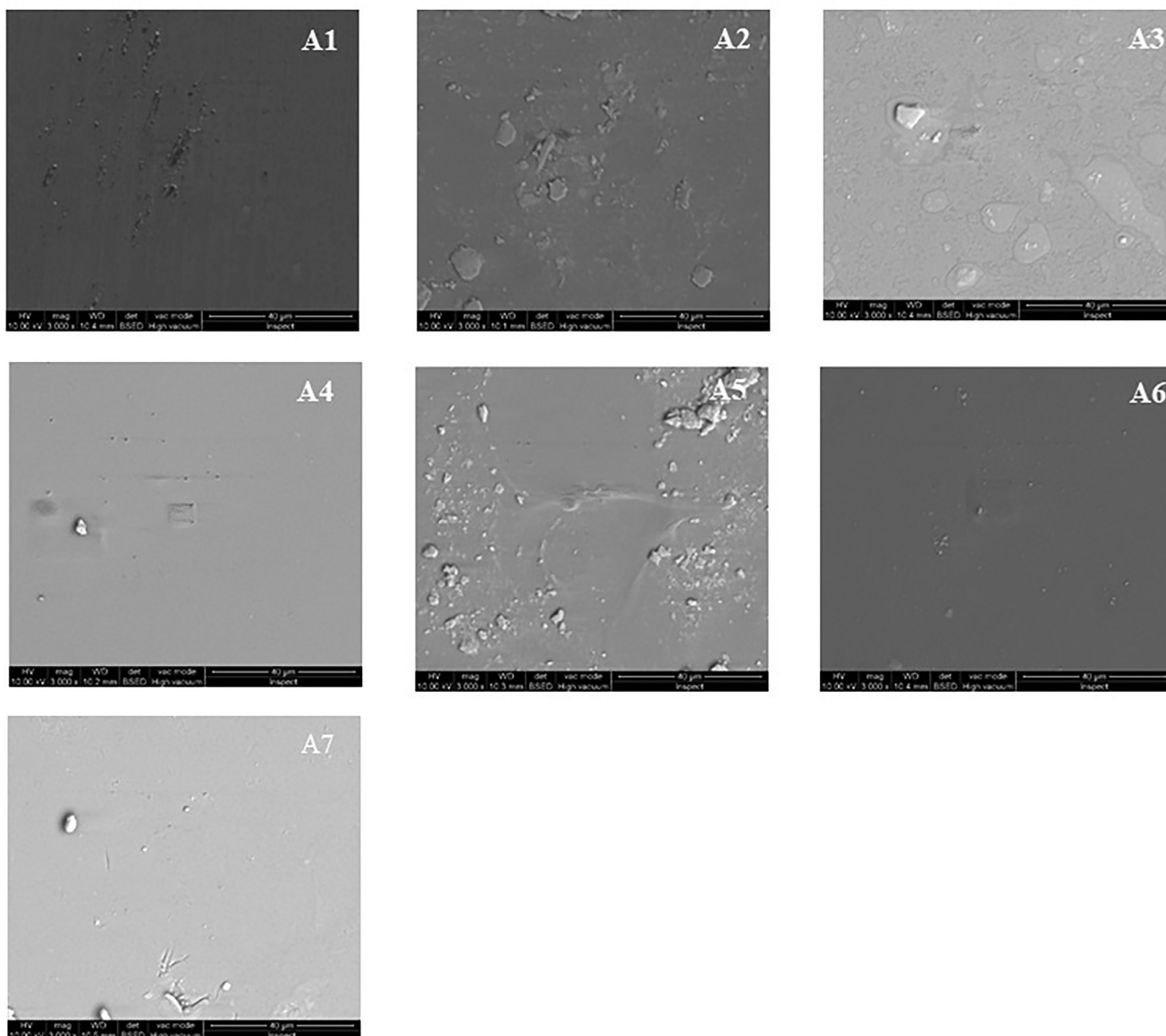


Fig. 11. SEM micrographs of SPEs films based on CMC/acetic acid.

in the free volume for ions motion through CMC backbone. Additionally, the linear relationship confirmed that the conductivity of the prepared SPEs obeys the Arrhenius theory [43,45]. This behavior of conductivity upon heating refers to that no phase changes or transitions taking place in the prepared polymer matrix. From the slope of this relation, the activation energy can be calculated using the Arrhenius equation:

$$\sigma_{ac} = \sigma_0 e^{-\frac{\Delta E}{RT}} \quad (5)$$

where, σ_{ac} is the AC conductivity, σ_0 is the pre-exponential factor, T is the absolute temperature, K is the Boltzmann constant and ΔE is the activation energy.

The relation between the activation energy and acid concentration is also presented in Fig. 12. From the Figure, it is obvious that the activation energy gradually decreased with increasing acid concentration to 5 wt.% due to the enhancement of ion density. However, at higher contents of acid, the activation energy is increased as the movement of ions has been impeded at higher acid contents. The values of the activation energy for the prepared SPEs are presented in Table 4. Additionally, it is clear from the figure that the conductivity is inversely proportional to the activation en-

ergy. Additionally, the values of activation energy agree with that of UV-Vis. and FTIR and confirmed that the sample A3 is the most suitable for application in electrochemical devices.

3.7.3. Dielectric results

Dielectric constant and dielectric loss (loss factor) are considered two of the most important physical quantities to discuss the electrical behavior of SPE films. Figs. 14 and 15 presents the variation has been occurred in both quantities for all studied samples. Both dielectric constant and dielectric loss are calculated using the following equations:

$$\varepsilon' = Cd/\varepsilon_0 A \quad (6)$$

$$\varepsilon'' = \sigma/\varepsilon_0 \omega \quad (7)$$

where, C is the capacitance of the SPEs under study, ε_0 is the permittivity of free space and ω is the angular frequency. It is clear from the figures that the sample named A3 has the highest dielectric constant and dielectric loss respectively in comparison with other samples.

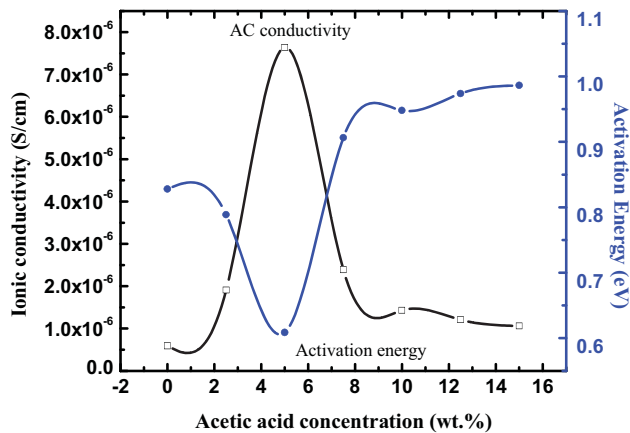


Fig. 12. The dependence of CMC-Gly- acetic acid SPEs ionic conductivity and activation energy on acetic acid concentration at room temperature.

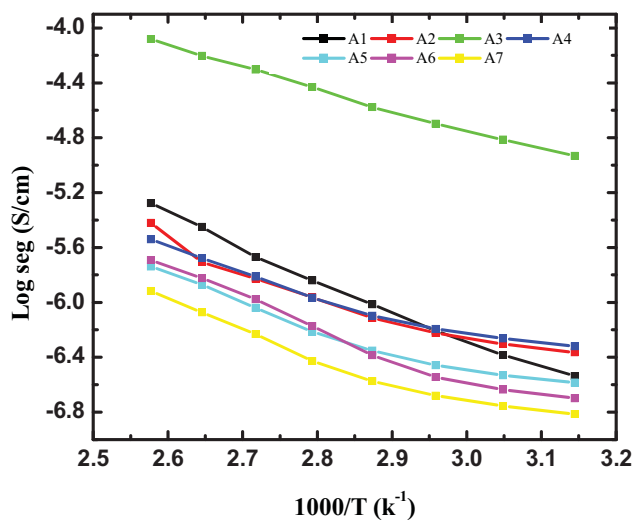


Fig. 13. Temperature dependence of AC conductivity for pure CMC and CMC doped with acetic acid.

The figures shows that, in the range of low frequencies, the values of both dielectric constant and dielectric loss are maximum but as the frequency starts to increase both dielectric constant and dielectric loss begins to decrease, and this phenomenon is observed at reasonable frequencies. However, in the high frequency range these two physical quantities are approximately constant. The reason for this change in both quantities with the change in frequency as mentioned before is that the dipoles keep track of the applied field direction at low frequencies. Where, the decrease in dielectric constant and dielectric loss at moderate frequencies happens as the dipoles do not have enough time to orient themselves quickly in the direction of the applied field so they begin to lag. However, at high frequencies the dipoles cannot orient themselves [40–44]. Furthermore, as for crystalline and semi-crystalline polymers, the crystalline regions dissolve progressively with frequency into amorphous regions and hence the number of charge carriers increases leading to the enhancement of conductivity. This behavior influences the dynamics of CMC and hence the CMC dielectrics.

3.8. Thermal analysis

Thermograms of TGA and its derivatives (DTG) for pure CMC and CMC-Gly-acetic acid are indicated in Fig. 16 and Fig. 17 respectively as a function of temperature. TGA curves and DTG results show that the thermal stability of the prepared films is changed

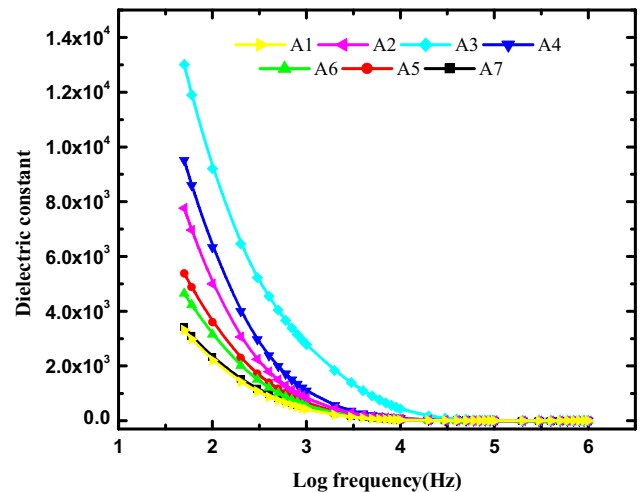


Fig. 14. Dielectric constant as a function of Log frequency for all studied samples.

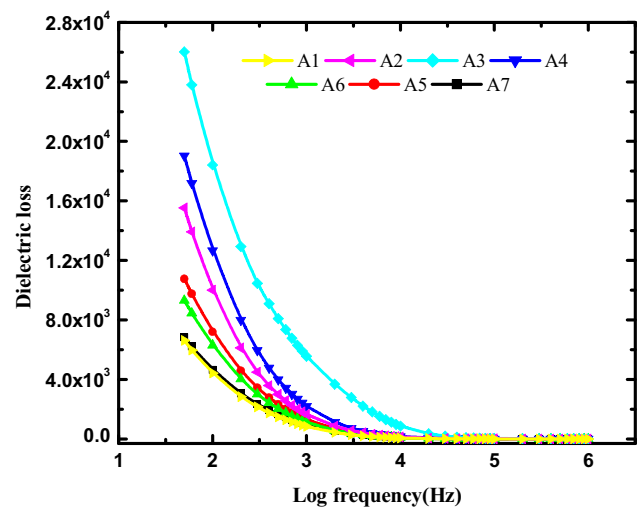


Fig. 15. Dielectric loss as a function of Log frequency for all SPE Samples.

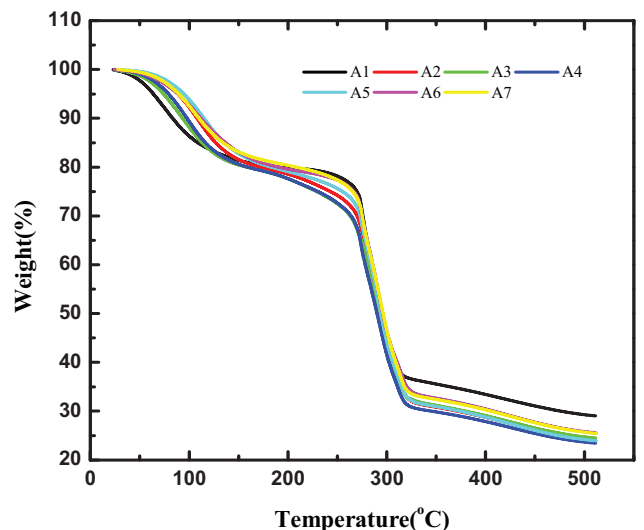


Fig. 16. TGA curves for all SPE films from ambient temperature to 511 °C.

Table 6

Thermal parameters of CMC and CMC doped with different percentages of acetic acid obtained from both TGA and Dr TGA analyzers.

Samples	TGA analyzer			Dr TGA analyzer	
	Stage no.	Weight loss (%)	Temperature range (°C)	DTG peaks(°C)	DTG minima (°C)
A1	1	19.13	31.69–168.30	308.05	89.14
	2	43.89	168.30–318.36	272.38	278.78
	3	7.64	318.36–508.68	404.15	
A2	1	19.95	38.50–158.77	267.44	119.75
	2	48.69	158.77–361.05	313.93	275.47
	3	7.14	361.05–509.04		
A3	1	19.72	41.10–170.75	267.53	103.24
	2	49.39	170.75–337.22	314.56	
	3	6.17	362.35–510.33		
A4	1	19.25	47.10–156.17	262.36	108.26
	2	50.1	156.17–334.62	311.86	274.67
	3	6.66	334.62–507.74		
A5	1	18.52	47.74–161.37	262.82	125.05
	2	50.12	161.37–339.82	315.21	
	3	7.14	339.82–509.04		
A6	1	19.48	34.60–181.29	272.59	119.82
	2	47.5	181.29–343.86	307.03	
	3	7.11	343.86–507.74	317.15	
A7	1	18.05	49.04–173.35	270.18	115.21
	2	48.46	173.35–335.92	314.42	
	3	7.37	335.92–507.74		

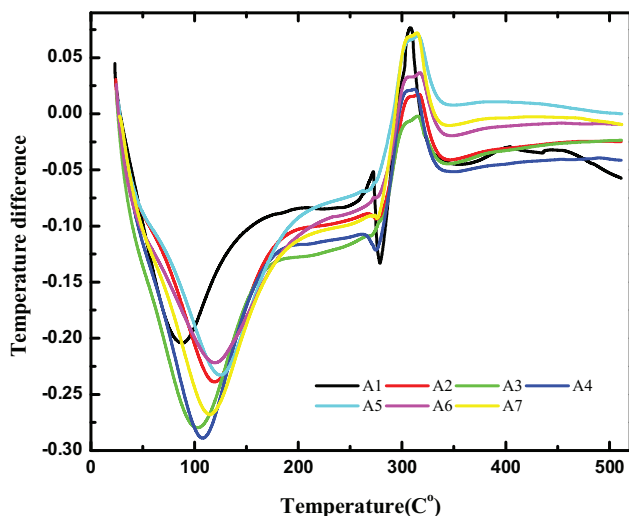


Fig. 17. DrTGA curves for all SPE films from ambient temperature to 511 °C.

with changing acid percentages as shown in Figs. 16 and 17. In the case of pure CMC three stages of weight loss are observed as shown in Fig. 16. The first loss in weight is about 19.13% in the temperature range from 31.69 to 168.30 °C. The initial loss in the weight is attributed to the presence of moisture in SPE films as polysaccharides have a strong ability to absorb water (moisture) from its surroundings [46,47]. The second weight loss is 43.89% in the temperature range from 168.30 to 318.36 °C and this loss is due to the loss of COO from the SPE films [47]. The rate at which the weight is being lost due to temperature increases follow the appropriate route as the temperature increases the final degradation causes loss in weight of 7.64% in the temperature range 318.36–508.68 °C which may be a result of the degradation of the material remaining into carbon residues. As a result of adding acetic acid, it is observed that there are also three stages of weight loss which also presented in Fig. 16 for sample A3 where the thermal stability increases. Table 6 presents the thermal behavior of different SPE films as a function of change in weight loss and its derivatives. Meanwhile, the different thermogravimetric parameters such

Table 7

Onset temperature as (°C), endset temperature as (°C) and the inflection point as (°C) of CMC and CMC doped with different concentrations of acetic acid obtained from both TGA and Dr TGA analyzers.

Structure	T _{onset}	T _{endset}	T _p
A1	44.5	332.3	87.1
A2	64.6	327.6	120.4
A3	53.8	324.3	103
A4	61.2	318.9	108.2
A5	74.7	327.6	125.2
A6	65.8	333.3	119.9
A7	69.1	328.7	114.6

as T_{onset}, T_{endset} and T_p are tabulated in Table 7. Where, T_{onset} refers to the extrapolated onset temperature that defines the temperature at which the weight loss begins while the weight loss finished is referred as T_{endset}. Meanwhile, the point of greatest rate of change on the weight loss curve that is known as the inflection point (T_p) is determined from the Dr TGA graph.

For more explanation, Dr TGA peak (first endothermic peak) for pure CMC appeared at lower temperatures than that for the doped samples which means that the CMC-Gly-acetic acid films are more stable. Moreover, the films are decomposed completely at around 100 °C which means that they are stable up to this temperature [47–49].

For electrochemical power applications (such as gas sensors, solar cells and batteries) and thermoplastic applications, the thermal stability is an important property as it reveals that CMC can be used as SPE [50].

4. Conclusion

Collecting the above data one can conclude the following point:

Based on UV- Vis results, the optical band gap of pure CMC is decreased with the addition of acetic acid and that the sample A3 possesses the lowest band gap.

FTIR results confirmed that the protons (H⁺) of the hydroxyl group (COOH) of acetic acid are dissociated and a strong interaction between CMC and acetic acid takes place. Where, the

characteristic bands of CMC are shifted to the higher wavenumber range.

The interaction of CMC and acetic acid was further identified by ¹HNMR, the obtained shifts confirming the results obtained by FTIR. SEM micrographs indicated that almost all samples are smooth and compact structure while only two samples were a little bit show sedimentation.

Electrical conductivity of CMC at room temperature is increased from 5.89E-07 S/cm to 7.64E-06 S/cm by increasing acetic acid concentration from 0 to 5 wt.% and decreased at higher concentrations. Highest electrical conductivity belongs to the sample containing 5 wt.% acetic acid and that the temperature dependence of CMC/acetic acid SPEs obeys the Arrhenius theory.

The decrease in both dielectric constant and dielectric loss with increasing frequency is attributed to electrode the polarization phenomena (EP).

TGA results showed that the thermal stability of CMC is increased because of acetic acid addition.

Finally, it is concluded that the plasticized SPEs based on CMC and acetic acid can be used in the fabrication of optoelectronic and electrochemical devices.

Declaration of Competing Interest

The authors declare that they have no known competing financial interests or personal relationships that could have appeared to influence the work reported in this paper.

References

- [1] M. Ibrahim, A.J. Hameed, A. Jalbout, Molecular Spectroscopic Study of River Nile Sediment in the Greater Cairo Region, *Appl. Spectrosc.* 62 (3) (2008) 306–311, doi:10.1366/000370208783759795.
- [2] K. Srivastava, P. Tandon, K. Sinha, A. Srivastava, J. Wang, Study of molecular structure and hydrogen bond interactions in dipfluzine-benzoic acid (DIP-BEN) cocrystal using spectroscopic and quantum chemical method, *Spectrochim. Acta A*. 216 (2019) 7–14, doi:10.1016/j.saa.2019.01.092.
- [3] M. Mazumder, R. Ahmed, A. Wajahat Ali, S. Jae Lee, SEM and ESEM techniques used for analysis of asphalt binder and mixture: a state of the art review, *Constr. Build. Mater* 18620 (2018) 313–329, doi:10.1016/j.conbuildmat.2018.07.126.
- [4] A. Fakhry, O. Osman, H. Ezzat, M. Ibrahim, Spectroscopic analyses of soil samples outside Nile Delta of Egypt, *Spectrochim. Acta A*. 168 (2016) 244–252, doi:10.1016/j.saa.2016.05.026.
- [5] F. Zhang, Q. Fu, T. Lü, H. Huang, T. He, Improved thermal fractionation technique for chain structure analysis of ethylene/ α -olefin copolymers, *Polymer (Guildf)* 43 (3) (2002) 1031–1034, doi:10.1016/S0032-3861(01)00657-7.
- [6] N.K. Kim, R.J.T. Lin, D. Bhattacharyya, Flammability and mechanical behaviour of polypropylene composites filled with cellulose and polymer based fibres: a comparative study, *Compos. Part A Appl. Sci. Manuf.* 100 (2017) 215–226, doi:10.1016/j.compositesa.2017.05.017.
- [7] G. Fadillah, Ozi A. Saputra, T.A. Saleh, Trends in polymers functionalized nanostructures for analysis of environmental pollutants, *Trends Environ. Anal. Chem.* 26 (2020) e00084 Article, doi:10.1016/j.teac.2020.e00084.
- [8] M. Ibrahim, O. Osman, Spectroscopic analyses of cellulose: fourier transform infrared and molecular modelling study, *J. Comput. Theor. Nanosci.* 6 (2009) 1054–1058, doi:10.6000/1929-5030.2014.03.03.3.
- [9] A. Omar, H. Ezzat, H. Elhaes, M.A. Ibrahim, Molecular modeling analyses for modified biopolymers, *Biointerface Res. Appl. Chem.* 11 (1) (2021) 7847–7859, doi:10.33263/BRIAC11.78477859.
- [10] D.P. Suhas, A.V. Raghu, H.M. Jeong, T.M. Aminabhavi, Graphene-loaded sodium alginate nanocomposite membranes with enhanced isopropanol dehydration performance via a pervaporation technique, *RSC Adv* 3 (2013) 17120–17130, doi:10.1039/C3RA42062K.
- [11] D.P. Suhas, T.M. Aminabhavi, A.V. Raghu, para-Toluene sulfonic acid treated clay loaded sodium alginate membranes for enhanced pervaporative dehydration of isopropanol, *Appl Clay Sci* 101 (2014) 419–429, doi:10.1016/j.clay.2014.08.017.
- [12] S.P. Dharupaneedi, R.V. Anjanapura, J.M. Han, T.M. Aminabhavi, Functionalized graphene sheets embedded in chitosan nanocomposite membranes for ethanol and isopropanol dehydration via pervaporation, *Ind Eng Chem Res* 53 (2014) 14474–14484, doi:10.1021/ie502751h.
- [13] A.S. Samsudin, W.M. Khairul, M.I.N. Isa, Characterization on the potential of carboxy methylcellulose for application as proton conducting biopolymer electrolytes, *J Non-Cryst Solids* 358 (8) (2012) 1104–1112, doi:10.1016/j.jnoncrysol.2012.02.004.
- [14] K.S. Ngai, S. Ramesh, K. Ramesh, J.C. Juan, A review of polymer electrolytes: fundamental, approaches and applications, *Ionics (Kiel)* 22 (8) (2016) 1259–1279, doi:10.1007/s11581-016-1756-4.
- [15] M. Hassan, K.R. Reddy, E. Haque, S.N. Faisal, S. G.hasemi, A.I. Minett, V.G. Gomes, Hierarchical assembly of graphene/ polyaniline nanostructures to synthesize free-standing supercapacitor electrode, *Compos. Sci. Technol* 98 (2014) 1–8, doi:10.1016/j.compscitech.2014.04.007.
- [16] M.N. Chai, M.I.N. Isa, Electrical characterization and ionic transport properties of carboxyl methylcellulose-oleic acid solid polymer electrolytes, *Int. J. Polym. Anal. Ch.* 18 (4) (2013) 280–286, doi:10.1080/1023666X.2013.767033.
- [17] S.J. Han, H. Lee, H.M. Jeong, B.K. Kim, A.V. Raghu, K.R. Reddy, Graphene modified lipophilically by stearic acid and its composite with low density polyethylene, *J Macromol. Sci. B* 53 (7) (2014) 1193–1204, doi:10.1080/00222348.2013.879804.
- [18] S.B. Aziz, Z.H.Z. Abidin, M.F.Z. Kadir, Innovative method to avoid the reduction of silver ions to silver nanoparticles in silver ion conducting based polymer electrolytes, *Phys Scripta* 90 (3) (2015) 035808, doi:10.1088/0031-8949/90/3/035808.
- [19] S.B. Aziz, T.J. Woo, M.F. Kadir, H. M.Ahmed, A conceptual review on polymer electrolytes and ion transport models, *J Sci-Adv Mater Dev* 3 (1) (2018) 1–17, doi:10.1016/j.jsamd.2018.01.002.
- [20] F.Z. Benabid, F. Zouai, Natural polymers: cellulose, chitin, chitosan, gelatin, starch, carrageenan, xylan and dextran, *Alger. J. Nat. Prod.* 4 (2016) 348–357, doi:10.5281/zenodo.199036.
- [21] K.R. Reddy, K.P. Lee, A.L. Gopalan, Novel electrically conductive and ferromagnetic composites of poly(aniline-co-aminonaphthalensulfonic acid) with iron oxide nanoparticles: synthesis and characterization, *J Appl. Polym. Sci.* 106 (2) (2007) 1181–1191, doi:10.1002/app.26601.
- [22] M. Ibrahim, O. Osman, Spectroscopic analyses of cellulose: fourier transform infrared and molecular modelling study, *J Comput Theor Nanos* 6 (5) (2009) 1054–1058, doi:10.1166/jctn.2009.1143.
- [23] H.P. Fink, P. Weigel, H.J. Purz, J. Ganster, Structure formation of regenerated cellulose materials from NMMO-solutions, *Prog Polym Sci* 26 (9) (2001) 1473–1524, doi:10.1016/S0079-6700(01)00025-9.
- [24] H. Kang, W. Liu, B. He, L.Ma D.Shen, Y. Huang, Synthesis of amphiphilic ethyl cellulose grafting poly (acrylic acid) copolymers and their self-assembly morphologies in water, *Polymer (Guildf)* 47 (23) (2006) 7927–7934, doi:10.1016/j.polymer.2006.09.017.
- [25] M.Y. Eo, H. Fan, Y.J. Cho, S.M. Kim, S.K. Lee, Cellulose membrane as a biomaterial: from hydrolysis to depolymerization with electron beam, *Biomater. Res.* 20 (1) (2016) 16, doi:10.1186/s40824-016-0065-3.
- [26] M.L.H. Rozali, A.S. Samsudin, M.I. N.Isa, Ion conducting mechanism of carboxy methylcellulose doped with ionic dopant salicylic acid based solid polymer electrolytes, *Int J Appl Sci Tech* 2 (4) (2012) 113–121.
- [27] A.K. Siddhanta, K. Prasad, R. Meena, G. Prasad, G.K. Mehta, M.U. Chhatbar, M.D. Oza, S. Kumar, N.D. Sanandhya, Profiling of cellulose content in Indian seaweed Species, *Bioresour Technol* 100 (24) (2009) 6669–6673, doi:10.1016/j.biortech.2009.07.047.
- [28] H. Huang, P. He, N. Hu, Y. Zeng, Electrochemical and electrocatalytic properties of myoglobin and hemoglobin incorporated in carboxymethyl cellulose films, *Bioelectrochemistry* 61 (1–2) (2003) 29–38, doi:10.1016/S1567-5394(03)00057-4.
- [29] M.P. Adinugraha, D.W. Marseno, Synthesis and characterization of sodium carboxymethylcellulose from cavendish banana pseudo stem (*Musa cavendishii* LAMBERT), *Carbohydr Polym* 62 (2) (2005) 164–169, doi:10.1016/j.carbpol.2005.07.019.
- [30] A.A. Menazea, A.M. Ismail, I.S. Elshamwi, The role of Li4Ti5O12 nanoparticles on enhancement the performance of PVDF/PVK blend for lithium-ion batteries, *J. Mater Res Tech.* 9 (3) (2020) 5689–5698, doi:10.1016/j.jmrt.2020.03.093.
- [31] A.A. Menazea, One-pot pulsed laser ablation route assisted copper oxide nanoparticles doped in PEO/PVP blend for the electrical conductivity enhancement, *J. Mater. Res. Technol* 9 (2) (2020) 2412–2422, doi:10.1016/j.jmrt.2019.12.073.
- [32] G.K. Prajapati, R. Roshan, P.N. Gupta, Effect of plasticizer on ionic transport and dielectric properties of PVA–H3PO4 proton conducting polymeric electrolytes, *J. Phys. Chem. Solids*. 71 (12) (2010) 1717–1723, doi:10.1016/j.jpcc.2010.08.023.
- [33] I.S. Elashmawi, A.A. Menazea, Different time's Nd:YAG laser- irradiated PVA/Ag nanocomposites: structural, optical, and electrical characterization, *J. Mat. Res. Tech.* 8 (2019) 1944–1951, doi:10.1016/j.jmrt.2019.01.011.
- [34] A.M. Abdelghany, E. M.Abdelrazek, D.S. Rashad, Impact of in situ preparation of CdS filled PVP nano-composite, *Spectrochim. Acta A* 130 (2014) 302–308, doi:10.1016/j.saa.2014.04.049.
- [35] E.A. Davis, N.F. Mott, Conduction in non-crystalline systems V. Conductivity, optical absorption and photoconductivity in amorphous semiconductors, *Phil. Mag* 22 (179) (1970) 0903–0922, doi:10.1080/14786437008221061.
- [36] K.K. Kumar, M. Ravi, Y. Pavani, S. Bhavani, A.K. Sharma, V.N. Rao, Investigations on the effect of complexation of NaF salt with polymer blend (PEO/PVP) electrolytes on ionic conductivity and optical energy band gaps, *Physica B* 406 (9) (2011) 1706–1712, doi:10.1016/j.physb.2011.02.010.
- [37] C. Rishi Pal, M. Suman, A.K. Tomar, K. Shyam, γ -Irradiated PVA/Ag nanocomposite films: materials for optical applications, *J. Alloys Compd.* 538 (2012) 212–219, doi:10.1016/j.jallcom.2012.05.085.
- [38] M. Yadoliahi, H. Namazi, Synthesis and characterization of carboxymethyl cellulose/layered double hydroxide nanocomposites, *J. Nanopart Res* 15 (2013) 1563, doi:10.1007/s11051-013-1563-z.
- [39] S.B. Aziz, M.A. Rasheed, A.M. Hussein, H.M. Ahmed, Fabrication of polymer blend composites based on [PVA-PVP](1-x):(Ag2S) x (0.01 \leq x \leq 0.03) with small optical band gaps: structural and optical properties, *Mater Sci Semicond Process* 71 (2017) 197–203, doi:10.1016/j.mssp.2017.05.035.

- [40] S.B. Aziz, O. Gh. Abdullah, A.M. Hussein, R.T. Abdulwahid, M.A. Rasheed, H.M. Ahmed, S.W. Abdalqadir, A.R. Mohammed, Optical properties of pure and doped PVA: PEO based solid polymer blend electrolytes: two methods for band gap study, *J Mater Sci: Mater Electron* 28 (2017) 7473–7479, doi:[10.1007/s10854-017-6437-1](https://doi.org/10.1007/s10854-017-6437-1).
- [41] M.N. Chai, M.I.N. Isa, Novel proton conducting solid bio-polymer electrolytes based on carboxymethyl cellulose doped with oleic acid and plasticized with glycerol, *Sci Rep* 6 (2016) 27328, doi:[10.1038/srep27328](https://doi.org/10.1038/srep27328).
- [42] M.L.H. Rozali, A.S. Samsudin, M.I.N. Isa, Ion conducting mechanism of carboxy methylcellulose doped with ionic dopant salicylic acid based solid polymer electrolytes, *Int. J Appl Sci Technol* 2 (4) (2012) 113–121, doi:[10.4028/www.scientific.net/AMR.1107.230](https://doi.org/10.4028/www.scientific.net/AMR.1107.230).
- [43] M. Tufan, E. Uraz, C. Tosun, H. Gerçel, Synthesis and characterization of carboxymethyl cellulose film from pistachio shells, *Int. J. Adv. Sc.Eng. Tech.* 4 (2016) 153–155.
- [44] M.A. Ramlli, M.I.N. Isa, Solid biopolymer electrolyte based carboxymethyl cellulose doped with ammonium fluoride: ionic transport and conduction mechanism, *Polym from Renewe Resour* 6 (2) (2014) 55–63, doi:[10.1177/204124791500600202](https://doi.org/10.1177/204124791500600202).
- [45] H. Huang, P. He, N. Hu, Y. Zeng, Electrochemical and electrocatalytic properties of myoglobin and hemoglobin incorporated in carboxymethyl cellulose films, *Bioelectrochemistry* 61 (1–2) (2003) 29–38, doi:[10.1016/S1567-5394\(03\)00057-4](https://doi.org/10.1016/S1567-5394(03)00057-4).
- [46] C. Dwivedi, I. Pandey, H. Pandey, P.W. Ramteke, A.C. Pandey, S.B. Mishra, S. Patil, Chapter 9, Electrospun nanofibrous scaffold as a potential carrier of antimicrobial therapeutics for diabetic wound healing and tissue regeneration, in: A.M. Grumezescu (Ed.), *Nano- and Microscale Drug Delivery Systems*, Elsevier Inc, 2017, pp. 147–164, doi:[10.1016/B978-0-323-52727-9.00009-1](https://doi.org/10.1016/B978-0-323-52727-9.00009-1).
- [47] S. El-Sayed, K.H. Mahmoud, A.A. Fatah, A.D.S.C. Hassen, DSC, TGA and dielectric properties of carboxymethyl cellulose/polyvinyl alcohol blends, *Physica B* 406 (21) (2011) 4068–4076, doi:[10.1016/j.physb.2011.07.050](https://doi.org/10.1016/j.physb.2011.07.050).
- [48] B. Kayyrapu, R. Chekuri, Thermal and Conductivity Studies of VO₂+ Doped Methacrylic Acid-Ethyl Acrylate (MAA: EA) Copolymer Films, *Mat. Res* 21 (1) (2018), doi:[10.1590/1980-5373-mr-2017-0328](https://doi.org/10.1590/1980-5373-mr-2017-0328).
- [49] D.R. Biswal, R.P. Singh, Characterisation of carboxymethyl cellulose and polyacrylamide graft copolymer, *Carbohydr. Polym.* 57 (4) (2004) 379–387, doi:[10.1016/j.carbpol.2004.04.020](https://doi.org/10.1016/j.carbpol.2004.04.020).
- [50] H. Ahmad, I. Kargarzadeh, I. Abdullah, A. Dufresne, S.Y. Zainudin, R.M. Sheltami, Effects of hydrolysis conditions on the morphology, crystallinity, and thermal stability of cellulose nanocrystals extracted from kenaf bast fibers, *Cellulose* 19 (3) (2012) 855–866, doi:[10.1007/s10570-012-9684-6](https://doi.org/10.1007/s10570-012-9684-6).